Molecular and Electronic Structure of Two Linear Thiophenolate-Bridged Heterotrinuclear Complexes $[LFeRuFeL]^{2+/3+}$ (L = 1,4,7-Tris(4-*tert*-butyl-2-mercaptobenzyl)-1,4,7-triazacyclononane)

Belen Albela,[a] Eckhard Bill,[a] Oliver Brosch,[a] Thomas Weyhermüller,[a] and Karl Wieghardt*[a]

Keywords: Thiolato-bridged complexes / Iron / Ruthenium / Mixed-valent compounds / Mössbauer spectroscopy

The reaction of $[Fe^{III}L]$ with $[Ru^{II}Cl_2(dmso)_4]$ in methanol under argon, affords, upon addition of $NaPF_6$, brown crystals of $[LFeRuFeL](PF_6)_2 \cdot 3\ CH_3OH$ (**1**). Its one-electron oxidation product $[LFeRuFeL](PF_6)_3$ (**2**) [L = 1,4,7-(4-*tert*-butyl-2-mercaptobenzyl)-1,4,7-triazacyclononane] was generated by using one equivalent of $[NO]BF_4$. The crystal structure determination of $[LFeRuFeL](BPh_4)_2 \cdot CH_3CN \cdot 3\ (CH_3)_2CO$ shows that **1** contains a trinuclear, face-sharing thiolato-bridged dication. Mössbauer spectroscopy established that the oxidation state distribution of **1** can best be described by $Fe^{2.5}Ru^{III}Fe^{2.5}$ and **2** by $Fe^{III}Ru^{III}Fe^{III}$. Complex **1** possesses a diamagnetic (S_t = 0) and **2** an S_t = 1/2 ground state. The electronic structures of **1** and **2** are rationalized by an MO picture involving Fe–Ru metal-metal bonds of bond order 0.5 in both species. Complex **1** is formally a mixed valence compound with complete delocalization of the "excess electron" (class III).

Introduction

In a series of papers[1−6] we have recently shown that mononuclear complexes of the type $[M^{III}L]$ (where L represents the trianionic ligand 1,4,7-tris(4-*tert*-butyl-2-mercaptobenzyl)-1,4,7-triazacyclononane and M = Fe, Ru) readily form homo- or heterotrinuclear complexes $[LM^1M^2M^1L]^{n+}$ with metal ions. These cations are isostructural, containing three face-sharing octahedra, namely two terminal $[M^1L]$ units comprising a *cis*-N_3S_3 donor set and a central MS_6 moiety. The three thiolato pendant arms of L form μ_2-thiolato bridges (Scheme 1). Complexes of this type have been shown to possess a rich redox chemistry where the isostructural tetra-, tri-, di- and monocationic species of a given transition metal ion combination are accessible via simple one-electron transfer steps. Thus it is possible to study magnetic exchange phenomena in paramagnetic species in a well-defined ligand matrix as a function of the local d^n electron configuration of the respective metal ion.

We have recently studied the complexes $[LFeFeFeL]^{2+/3+}$ [3] and their homologs $[LRuRuRuL]^{2+/3+}$.[5] It was shown that the two isoelectronic dications display an S_t = 1 ground state in the case of the tri-iron species but an S_t = 0 ground state for the triruthenium species. In contrast, both trications have an S_t = 1/2 ground state. In order to obtain a better understanding of their electronic structure, we decided that it would be of value to investigate the isoelectronic *hetero*trinuclear analogs $[LFeRuFeL]^{2+/3+}$. Here we report the synthesis, the molecular and electronic structures, and spectroscopic characterizations of these cations.

[a] Max-Planck-Institut für Strahlenchemie,
Stiftstrasse 34−36, D-45470 Mülheim an der Ruhr, Germany
Fax: (internat.) + 49(0)208/306-3952

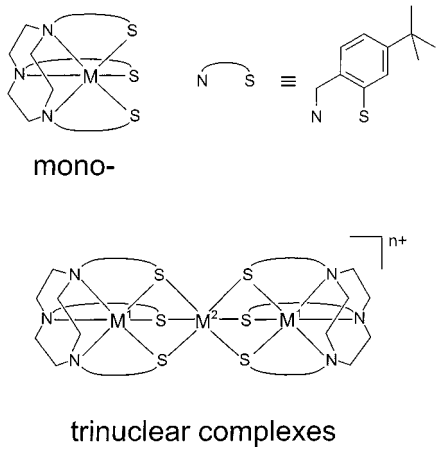

Scheme 1. Schematic structures of ML and $[\{M^1L\}_2M^2]^{n+}$ complexes

Results

Preparation of Complexes

Reaction of the mononuclear species $[Fe^{III}L]$[1][2] with $[Ru^{II}Cl_2(dmso)_4]$ (dmso = dimethyl sulfoxide) in the ratio 1:1 in methanol, under argon, at elevated temperatures, produced a clear, dark brown solution from which, upon addition of $NaPF_6$, brown microcrystals of $[LFeRuFeL](PF_6)_2 \cdot 3\ CH_3OH$ (**1**) were obtained. Recrystallization of this material from acetone/acetonitrile (1:1) and addition of $Na[BPh_4]$ afforded single crystals of $[\{LFe\}_2Ru](BPh_4)_2 \cdot CH_3CN \cdot 3\ (CH_3)_2CO$.

When the above reaction mixture was cooled, treated with one equivalent of $[NO]BF_4$, and stored at 4°C, brown microcrystals of $[LFeRuFeL](PF_6)_3$ (**2**) were obtained after addition of $NaPF_6$. Complex **2** is the one-electron oxidized form of **1**.

  1434−1948/00/0101−0139 $ 17.50+.50/0

Electronic spectra of solutions **1** and **2** in CH_3CN are displayed in Figure 1. The spectrum of **1** shows absorption maxima λ_{max} (ε, $L \cdot mol^{-1} \cdot cm^{-1}$) at 365 sh (ca. $9.5 \cdot 10^3$), 475 ($4.1 \cdot 10^3$), 670 sh ($2.0 \cdot 10^3$), 830 ($1.9 \cdot 10^3$), 1320 nm ($3.6 \cdot 10^3$); for **2** these values are at ca. 420 sh ($1.2 \cdot 10^4$), ca. 550 sh ($4.7 \cdot 10^3$), ca. 620 sh ($3.2 \cdot 10^3$), 750 sh ($2.0 \cdot 10^3$). Clearly, the intense band at 1320 nm in the spectrum of **1** is an intervalence charge transfer band (see below) since it is absent in the spectrum of **2**.

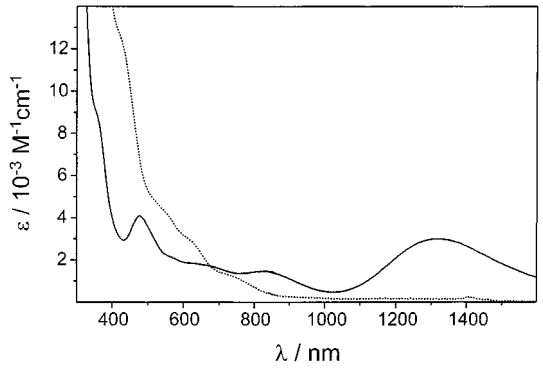

Figure 1. Electronic spectra of **1** (−) and **2** (---) in CH_3CN

The cyclic and square-wave voltammograms of **1** and **2** measured in CH_3CN (0.10 M $[N(nBu)_4]PF_6$) at 293 K are identical and are shown in Figure 2. Three reversible one-electron transfer processes are observed at $E^1_{1/2} = 1.09$ V vs ferrocenium/ferrocene (Fc^+/Fc), $E^2_{1/2} = -0.07$ V vs Fc^+/Fc, and $E^3_{1/2} = -1.07$ V vs Fc^+/Fc which are assigned as depicted in Equation 1.

$$[LFeRuFeL]^{4+} \underset{+e}{\overset{-e}{\rightleftharpoons}} [LFeRuFeL]^{3+} \underset{+e}{\overset{-e}{\rightleftharpoons}} [LFeRuFeL]^{2+} \underset{+e}{\overset{-e}{\rightleftharpoons}} [LFeRuFeL]^{1+} \quad (1)$$

Reduction of the dication to the monocation is only reversible on the time-scale of a CV experiment; it decomposes to $[Fe^{II}L]^-$ and (probably) $[Ru^{II}(NCCH_3)_6]^{2+}$ at slower scan rates. The small peaks at −0.75 V and +0.60 V vs Fc^+/Fc correspond to the [FeL]/$[FeL]^-$ and $[Ru^{III}(NCCH_3)_6]^{3+/2+}$ couple, respectively.

Magnetic Susceptibility and EPR Spectroscopy

Temperature-dependent magnetic-susceptibility measurements in the range 2−298 K were performed on a SQUID magnetometer in a field of 1 T. The raw data were corrected for underlying diamagnetism by using Pascal's tabulated constants. Temperature-independent paramagnetism (TIP), χ_{TIP}, is a fit parameter.

Figure 3 shows the calculated effective magnetic moments as a function of the temperature for **1** (top) and **2** (bottom). For complex **1**, μ_{eff} varies from 0.59 μ_B at 2 K to 1.97 μ_B at 290 K, which is predominantly due to TIP ($\chi_{TIP} \approx 2.0 \cdot 10^{-3}$ cm^3 mol^{-1}). Thus **1** has a diamagnetic $S_t = 0$ electronic ground state. A small amount of a paramagnetic impurity (< 2%) is also present in the sample of **1**.

The temperature-dependence of the effective magnetic moment of **2** was satisfactorily modeled for an $S_t = 1/2$ ground state with the following parameters: $g = 2.11$; $\chi_{TIP} = 1380 \cdot 10^{-6}$ cm^3 mol^{-1}. Note that large TIP values have been found for all trinuclear complexes of the type $[LFeMFeL]^{n+}$ (M = Cr, Co, Fe, Ni).[3−6]

The $S_t = 1/2$ ground state of **2** has been confirmed by its X-band EPR spectrum in CH_3CN solution at 10 K, which is shown in Figure 4. An axial signal with $g_\perp = 2.31$ and $g_\parallel = 1.86$ has been observed. The average $g^{av} = 2.16$ is

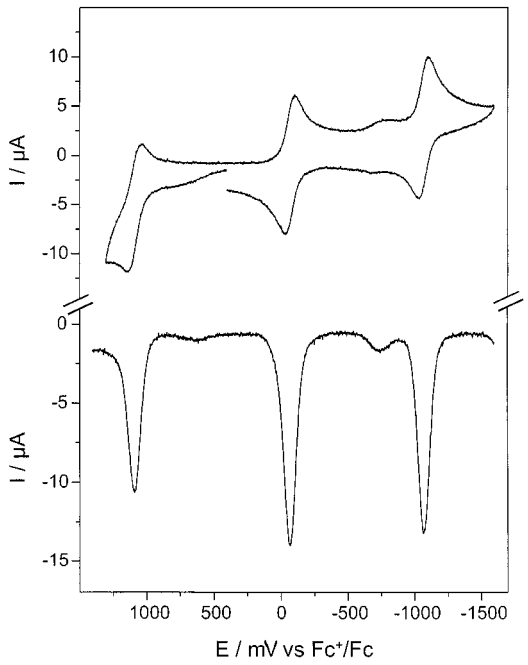

Figure 2. Cyclic (top) and square-wave (bottom) voltammogram of **1** at 298 K in CH_3CN (0.10 M $[N(nBu)_4]PF_6$, glassy carbon electrode, scan rate *cv* 100 mV s^{-1}; pulse height *sw* 25 mV, frequency 30 Hz)

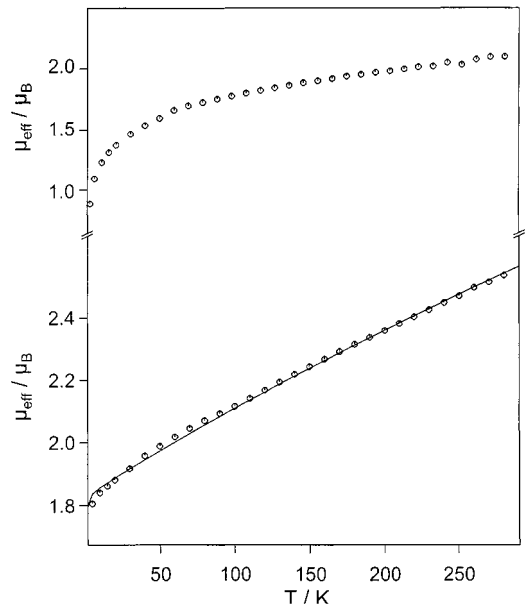

Figure 3. Temperature-dependence of the magnetic moment μ_{eff}/μ_B of solid **1** (top) and **2** (bottom); the solid line represents a fit; see text for parameters

in good agreement with that obtained from susceptibility measurements. Complex **1** is EPR-silent.

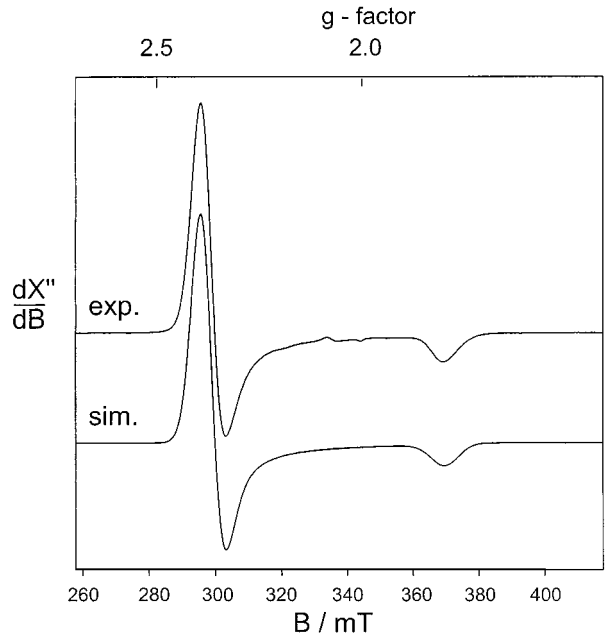

Figure 4. X-band EPR spectrum of **2** in frozen CH_3CN at 10 K and simulation (frequency 9.64 GHz; power 0.05 mW; modulation amplitude 11.4 G; modulation frequency 100 kHz)

Crystal Structure Determination

Crystals of $[LFeRuFeL](BPh_4)_2 \cdot CH_3CN \cdot 3\,(CH_3)_2CO$ consist of well-separated dications $[LFeRuFeL]^{2+}$ and tetraphenylborate anions together with acetonitrile and acetone molecules of crystallization. Figure 5 shows different views of the dication and Table 1 summarizes bond lengths and angles of the trinuclear core. The dication consists of three face-sharing thiolato-bridged octahedra with two terminal iron ions and a central ruthenium ion. The stereochemistry of these trinuclear cations, $[\{LM^1\}_2M^2]^{n+}$, has been discussed previously.[3,5,6] The staggered configuration of the six tertiary butyl groups (looking down the Fe···Ru···Fe axis) in the achiral stereoisomer $\Delta(\lambda\lambda\lambda)\cdots\Lambda(\delta\delta\delta)$ yields a stable structure which has been observed in all cases where the M1···M2 distance is >2.9 Å. Only in $[LRuRuRuL](PF_6)_2 \cdot H_2O$ has the $\Delta(\lambda\lambda\lambda)\cdots\Delta(\lambda\lambda\lambda)$ [and its enantiomer $\Lambda(\delta\delta\delta)\cdots\Lambda(\delta\delta\delta)$] diastereomer been observed.[5] In this case, the six tertiary butyl groups are eclipsed and the Ru−Ru distance is at 2.775 Å. The dication in **1** adopts the achiral $\Delta(\lambda\lambda\lambda)\cdots\Lambda(\delta\delta\delta)$ configuration. The ruthenium ion is located on a crystallographic inversion center. The average Fe−N and Fe−S bond lengths at 2.061(4) and 2.251(4) Å are indentical to those observed in all other structure containing an $[LFeMFeL]^{n+}$ cation.[1−6] Interestingly, the three crystallographically independent Ru−S distances of the central RuS_6 moiety are not quite equivalent. There are two longer Ru−S distances at 2.368(1) Å and a shorter one at 2.350(1) Å (tetragonally compressed octahedron). The Fe···Ru distance at 2.804(1) Å is short and may indicate the onset of direct metal−metal bonding. In $[LRuRuRuL]^{2+}$ the Ru−Ru distance is found at 2.775(1) Å[5] and in $[LFeFeFeL]^{2+}$ the Fe···Fe distance is 2.848(1) Å.[3]

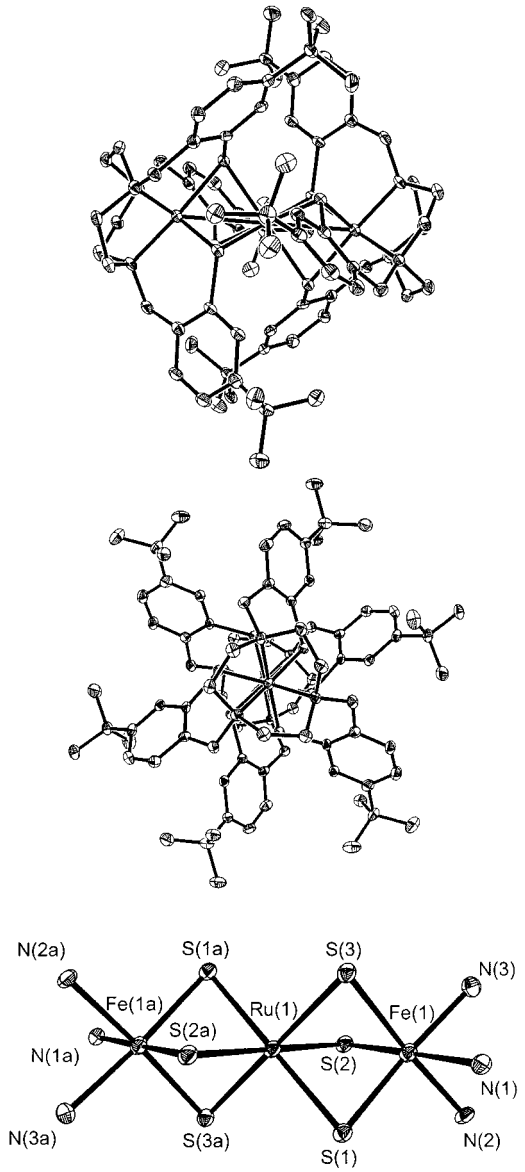

Figure 5. Structure of the dication in crystals of $[LFeRuFeL](BPh_4)_2 \cdot CH_3CN \cdot 3\,(CH_3)_2CO$: a) side-view, b) view down the Fe···Ru···Fe axis, and c) view of the core structure with atom labels

Mössbauer Spectroscopy

Complexes **1** and **2** have been studied by ^{57}Fe-Mössbauer spectroscopy in zero and applied fields. For both compounds, the zero-field spectra recorded on solid material at 80 K are single quadrupole doublets that could be fitted with Lorentzian lines as shown in Figure 6. The two local iron sites in **1** and **2** are indistinguishable; the parameters are summarized in Table 2. Since the same behavior is

Table 1. Selected bond lengths [Å] and angles [deg] for $[LFeRuFeL](BPh_4)_2 \cdot CH_3CN \cdot 3\,(CH_3)_2CO$ (**1**)

Ru(1)−S(1)	2.3502(12)	Fe(1)−N(1)	2.065(4)
Ru(1)−S(2)	2.3661(12)	Fe(1)−N(2)	2.059(4)
Ru(1)−S(3)	2.3696(14)	Fe(1)−N(3)	2.060(4)
Ru(1)−Fe(1)	2.8038	Fe(1)−S(1)	2.247(2)
		Fe(1)−S(2)	2.249(2)
		Fe(1)−S(3)	2.256(2)
S(1)−Ru(1)−S(2)	84.46(4)	N(2)−Fe(1)−N(3)	84.1(2)
S(1)−Ru(1)−S(2)′	95.54(4)	N(2)−Fe(1)−N(1)	84.7(2)
S(1)′−Ru(1)−S(3)	94.80(5)	N(3)−Fe(1)−N(1)	84.5(2)
S(2)′−Ru(1)−S(3)	96.88(5)	N(2)−Fe(1)−S(1)	93.21(12)
S(1)′−Ru(1)−S(3)′	85.20(5)	N(1)−Fe(1)−S(1)	91.40(12)
S(2)′−Ru(1)−S(3)′	83.12(5)	N(2)−Fe(1)−S(2)	92.65(12)
S(1)′−Ru(1)−S(2)′	84.46(5)	N(3)−Fe(1)−S(2)	94.30(12)
S(1)′−Ru(1)−S(2)	95.54(4)	S(1)−Fe(1)−S(2)	89.69(5)
S(1)−Ru(1)−S(3)	85.20(5)	N(3)−Fe(1)−S(3)	92.28(12)
S(2)−Ru(1)−S(3)	83.12(5)	N(1)−Fe(1)−S(3)	94.16(11)
S(1)−Ru(1)−S(3)′	94.80(5)	S(1)−Fe(1)−S(3)	90.39(5)
S(2)−Ru(1)−S(3)′	96.88(5)	S(2)−Fe(1)−S(3)	88.44(5)

found for the measurements at liquid helium temperatures, we can exclude the possibility of dynamic processes like valence detrapping playing a role. The ^{57}Fe-Mössbauer parameters of **1** and **2** clearly show that the redox states of the complexes are related to the iron oxidation states. The higher isomer shift and the lower quadrupole splitting of **1** indicates the more ferrous character of iron in **1** than in **2**. The iron ions in both **1** and **2** are low-spin.

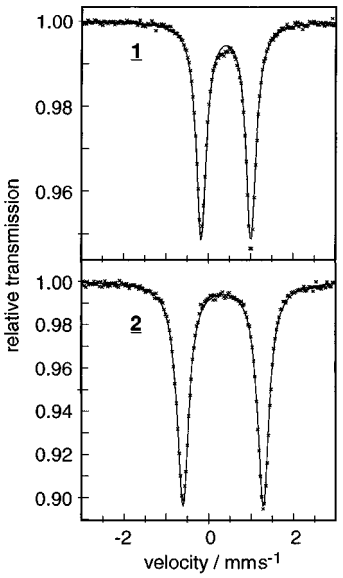

Figure 6. Zero-field Mössbauer spectra of crystalline samples of **1** and **2** measured at 80 K. The solid lines are a fit with Lorentzian lines with isomer shift, quadrupole splitting and line width (fwhm) of (**1**: $\delta = 0.41$ mm s^{-1}, $\Delta E_Q = 1.18$ mm s^{-1}, $\Gamma = 0.33$ mm s^{-1}) and (**2**: $\delta = 0.34$ mm s^{-1}, $\Delta E_Q = 1.83$ mm s^{-1}, $\Gamma = 0.33$ mm s^{-1}). The small difference in isomer shift relative to the 4.2 K values given in Table 2 originates from the second-order Doppler shift

The Mössbauer parameters of **1** and **2** fit perfectly in a $\delta/\Delta E_Q$ correlation diagram (Figure 7A) that we have previously established for a series of isostructural complexes with the same $[FeMFe]^{n+}$ core where M is Cr, Fe, or Co. The terminal iron sites thus have variable formal oxidation states, which depend on the cluster oxidation state and on

Table 2. Mössbauer parameters for complexes **1** and **2**

Complex Complex	δ[a] [mm s^{-1}]	ΔE_Q,[b] [mm s^{-1}]	η[c]	S_t[d]	$\bar{\bar{A}}/\mu_N g_N$ [T][e]
1	0.43	+1.23	0.3	0	−
2	0.34	+1.83	0.2(1)	1/2	−3.07, −3.07, +1.76

[a] Isomer shift (4.2 K). − [b] Quadrupole splitting (4.2 K). − [c] Asymmetry parameter. − [d] Spin ground state. − [e] Magnetic hyperfine tensor.

the degree of valence delocalization mediated via the central MS_6 unit.[3] If we take these compounds as a reference series (Table 3) we can determine the iron valences of **1** and **2**. In particular, the Mössbauer isomer shift is a sensitive parameter for this purpose because it is a measure of the charge density at the iron nucleus. The apparently linear correlation of oxidation state and isomer shift shown in Figure 7B reveals an iron oxidation state of 2.9 for **2** (≈ +III) and an intermediate value of 2.5 for the reduced analogue **1**. Therefore the central ruthenium ion in this system must be persistently close to the trivalent state (+III) and

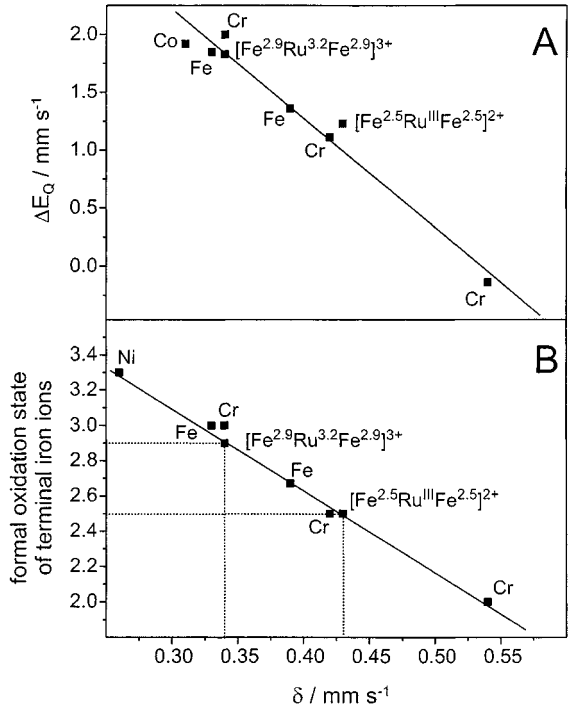

Figure 7. (A) Plot of the quadrupole splitting and ^{57}Fe-Mössbauer isomer shift for **1** and **2** together with the values of related complexes with the $[FeMFe]^{n+}$ core, M = Cr, Fe, Co, Ni taken from ref.[3][6] − (B) Correlation of the formal oxidation state and isomer shift for the same set of compounds. The dotted lines show the determination of this oxidation state for the iron ions in **1** and **2**, respectively

is not affected by the 2+/3+ redox transition of the cluster.

For diamagnetic compound **1**, the sign of V_{zz}, the main component of the electric field gradient (efg), and the asymmetry parameter η of the efg were determined from the Mössbauer spectrum, measured from a crystalline sample

Table 3. Summary of Mössbauer Parameters (4.2 K) of Complexes $[LFeMFeL]^{n+}$

Complex	ref.	δ[a] mm s^{-1}	ΔE_Q[b] mm s^{-1}	S_t[c]	Oxidation state of terminal iron ions
$[FeRuFe]^{2+}$	this work	0.43	+1.23	0	2.5
$[FeRuFe]^{3+}$	this work	0.34	+1.83	1/2	3.0
$[FeCrFe]^{1+}$	[3]	0.54	−0.14	$^3/_2$	2.0
$[FeCrFe]^{2+}$	[3]	0.42	+1.11	2	2.5
$[FeCrFe]^{3+}$	[3]	0.34	+2.00	1/2	3.0
$[FeCoFe]^{3+}$	[3]	0.31	+1.92	1	3.0
$[FeFeFe]^{2+}$	[3]	0.39	+1.36	1	2.67
$[FeFeFe]^{3+}$	[3]	0.33	+1.85	1/2	3.0
$[FeNiFe]^{3+}$	[6]	0.31	+0.52	1/2	3.0
$[FeNiFe]^{4+}$	[6]	0.26	+1.85	0	3.3

[a] Isomer shift of the terminal iron ions. − [b] Quadrupole splitting of the terminal iron ions. − [c] Electronic ground state of the trinuclear cation.

with an applied field of 7 T at 4.2 K (Figure 8). The spectrum could be readily simulated with the usual nuclear Hamiltonian[7][8] for the external field and a vanishing internal field. The sign of V_{zz} is found to be positive with η = 0.3. The parameters are summarized in Table 2.

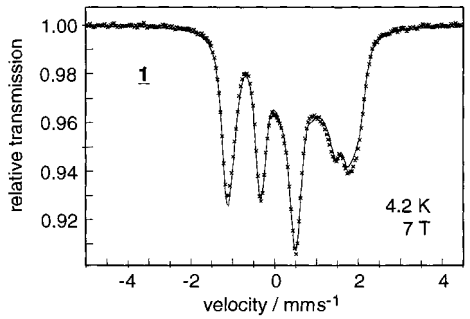

Figure 8. Magnetically perturbed Mössbauer spectrum of **1** measured at 4.2 K with a field B = 7 T applied perpendicular to the γ-rays. The solid line is a simulation for a diamagnetic system (zero internal field); the parameters are given in Table 2

Figure 9 shows the magnetic Mössbauer spectra of solid complex **2** recorded with applied fields of 4 T and 7 T at 4.2 K and 120 K. The spin ground state S_t = 1/2 of complex **2** is well separated from the excited states and the limit of strong coupling ($J >> \mu_B B$, kT) is valid even at 120 K according to the static magnetic susceptibility measurement. We have therefore used an effective spin Hamiltonian for the description of the magnetic Mössbauer spectra.[3] At liquid helium temperatures the spectra were simulated in the slow relaxation limit whereas at 120 K fast relaxation prevails. To limit the number of free parameters the g factors were fixed to the values determined from EPR. The sign of V_{zz} is unambiguously positive, as is clearly shown by the 120 K measurement, and the asymmetry parameter is 0.2(1). This result discloses the order of the 1e and a_1 iron 3d orbitals in the trigonal symmetry (t_{2g} in O_h symmetry).[3][9] The positive V_{zz} is consistent with a large positive valence electron contribution to the efg which is expected for an $(1e)^4(a_1)^1$ electron configuration if the 1e orbital set is lower in energy than the a_1 orbital.

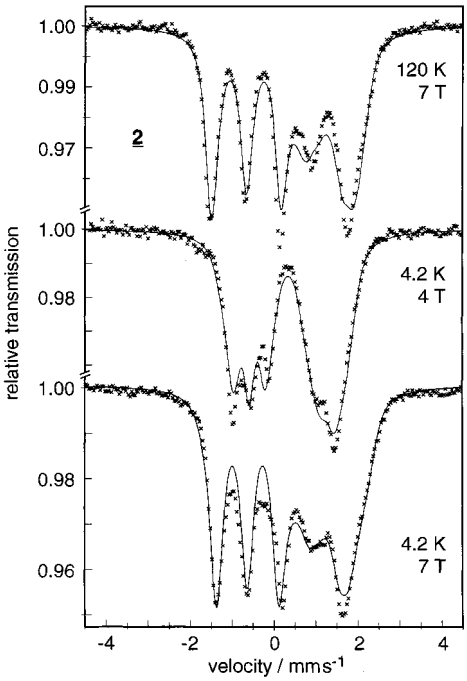

Figure 9. Magnetically perturbed Mössbauer spectrum of **2** measured at 4.2 K and 120 K with the indicated fields applied perpendicular to the γ-rays. The solid lines are a simulation for a system spin S_t = 1/2; the parameters are given in Table 2

Surprisingly, the fits required a finite value of the asymmetry parameter η = 0.2(1), and an Euler angle β = 22° which orients the principal z'-axis of the efg off from the principal z'-axis of the g and A tensors. The deviation is in contrast to the anticipated C_{3v} symmetry of the complex. A close inspection of the molecular structure shows a small distortion of the local iron sites in the crystal. There are two slightly longer Fe−S bonds [Fe(1)−S(3) and Fe(1)−S(3)′] and the RuS_6 octahedron shows a tetragonal compression with two shorter Ru−S bonds [Ru(1)−S(1) and Ru(1)−S(1)′].

The internal magnetic field induced by the total spin (S_t = 1/2) of the complex has a relatively small isotropic contribution and large anisotropy as shown by the trace and the components of the hyperfine coupling tensor given in Table 2 ($1/3\mathrm{Tr}(A)/g_N\beta_N$ = −1.46 T). This closely resembles the magnetic properties of iron in the corresponding $[FeFeFe]^{3+}$ complex.[3] The asymmetry owes its origin to significant spin-dipolar contributions to the A tensor, due to spin-orbit interaction in the $3d^5$ configuration of the low-spin Fe^{III}. The sign of the isotropic contribution to A is negative as it is for usual mononuclear iron compounds. This demonstrates that the local spins of the iron ions are parallel to the cluster spin, whereas the Ru^{III} spin is antiparallel, giving rise to the $|S_t = 1/2, S^* = 1>$ ground state. The A-tensor components given with respect to the total spin can be converted into local values related to the iron spin by using the spin projection factor derived from an application of the Wigner-Eckart theorem: $A_{(S_t=1/2)} = 2/3\ a_{S=1/2}$.

The obtained local values are $a_{S = 1/2}/g_N\mu_N$ = (−4.61, −4.61, +2.65) T.

In summary, Mössbauer spectroscopy allows one to experimentally determine the formal oxidation state of the iron ions in $[LFeMFeL]^{n+}$ complexes. As shown in Figure 7A, the isomer shift and the quadrupole splitting parameters of all complexes of this type reported to date are linearly correlated, and the corresponding data of **1** and **2** are in excellent agreement with this correlation. We have conclusively shown[3] that the iron ions in $[LFeCr^{III}FeL]^{3+}$ are purely low-spin ferric ions (oxidation state +III), whereas in $[LFeCr^{III}FeL]^{1+}$ they are low-spin ferrous (+II) and in $[LFeCr^{III}FeL]^{2+}$ are a mixed valent species with delocalized electronic structure (two $Fe^{2.5}$ ions). A plot of the corresponding ^{57}Fe-isomer shift vs the formal oxidation state is again linear, as displayed in Figure 7B. Using this correlation, an oxidation state of 2.9 (≈ +III) for **2** and of 2.5 for **1** is determined for the respective iron ions. Thus, **1** may be described as a $[LFe^{2.5}Ru^{III}Fe^{2.5}L]^{2+}$ and **2** as a $[LFe^{III}Ru^{III}Fe^{III}L]^{3+}$ species. In this manner we have established that the reduction of **2** by one-electron, yielding **1**, affects only the iron ions, and that both **1** and **2** contain a central Ru^{III} ion. Furthermore, the observation in the ^{57}Fe-Mössbauer spectrum of **1** of only a single iron site − even at 4.2 K − renders the dication a mixed valent species with a completely delocalized "excess" electron (class III according to Robin and Day[10]); the alternative formulation of **1** as a $[LFe^{III}Ru^{II}Fe^{III}L]^{2+}$ species is clearly ruled out by its Mössbauer spectra.

Discussion

In the preceding section it has been experimentally established that the cation $[LFeRuFeL]^{3+}$ in complex **2** contains two low-spin ferric ions with an $(1e)^4(a_1)^1$ local electron configuration and a central low-spin Ru^{III} ion, probably also with an $(1e)^4(a_1)^1$ configuration. The S_t = 1/2 ground state can then be rationalized by a MO description invoking two weak Fe−Ru bonds. The formation of three-center MOs by overlap of metal t_{2g} orbitals (specifically the a_1 orbitals) having lobes along the threefold symmetry axis, yields a bonding σ_b, a nonbonding σ_n, and an antibonding σ_a molecular orbital.[11][12] There are three electrons to occupy these MOs, σ_b^2 and σ_n^1, yielding an S_t = 1/2 ground state (Scheme 2). In the structurally characterized species $[Ru_3Cl_8(PEt_3)_4][SbF_6]$[13] a Ru−Ru distance at 2.91 Å has been found and a formal Ru−Ru bond order of 0.5 has been proposed. Analogously, an Fe−Ru bond of bond order 0.5 can be envisaged in $[LFeRuFeL]^{3+}$ (as in its previously described isoelectronic homotrinuclear species $[LRu^{III}Ru^{III}Ru^{III}L]^{3+}$).[5]

It is interesting that the isoelectronic species $[LFe^{III}Fe^{III}Fe^{III}L]^{3+}$ containing a low-spin central and two low-spin terminal ferric ions also possesses an S_t = 1/2 ground state.[3] The Fe···Fe distance has been determined at 2.86(2) Å by EXAFS spectroscopy or 2.79(2) Å from a low-quality X-ray crystal structure. The observed very strong antiferromagnetic coupling (J_a < −400 cm^{-1}) has been rationalized as originating from direct exchange between local a_1-orbitals and the onset of metal−metal bonding.

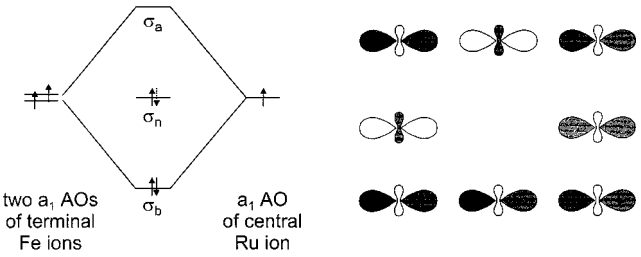

Scheme 2. Schematic MO representation for $[\{LFe\}_2Ru]^{2+/3+}$

Mössbauer spectroscopy unequivocally demonstrates that one-electron reduction of **2** to **1** affects only the two terminal iron ions which are on the time scale of this spectroscopy equivalent: $[LFe^{2.5}Ru^{III}Fe^{2.5}L]^{2+}$. The Ru−Fe distance at 2.804(1) Å is in the range where direct metal−metal bonding is certainly a possibility. The MO scheme (Scheme 2) immediately implies that the "excess" electron occupies the σ_n MO, giving rise to an electron configuration $\sigma_b^2\sigma_n^2$ where the Fe−Ru bonds also have a BO of 0.5 and the dication adopts a diamagnetic ground state. Similarly, $[LRuRuRuL]^{2+}$ has been shown to possess an S_t = 0 ground state and a relatively short Ru−Ru distance at 2.775(1) Å.[5]

On the other hand, isoelectronic $[LFeFeFeL]^{2+}$ possesses an S_t = 1 ground state[3] with no thermally accessible excited spin states. The Fe···Fe distance has been determined to be 2.848(2) Å which is slightly, but significantly, longer than in **1** or $[LRuRuRuL]^{2+}$. From Mössbauer spectroscopy, a fractional oxidation state of +2.67 for each of the three iron ions has been determined. The positive sign of the quadrupole splittings indicated that the local a_1-orbitals are the magnetic orbitals. The origin of the S_t = 1 ground state has been rationalized by a double exchange mechanism over three metal centers (Scheme 3). Only parallel alignment of the three respective local spins allows the excess electron to be transferred over all *three* metal centers. The negative sign of the effective Mössbauer hyperfine coupling constants A_i^{iso} indicates positive spin density at the central *and* terminal centers, thereby corroborating the above picture.[3] In this instance Fe···Fe metal bonding does not play a significant role, but delocalization of the excess electron via a double exchange mechanism enforces the above triplet ground state.

Finally, for the isoelectronic species $[LFe^{III}Co^{III}Fe^{III}L]^{3+}$, the observed S_t = 1 ground state[3] is thought to be attained via strong intramolecular ferromagnetic exchange coupling between two localized low-spin ferric ions which is mediated by a low-spin Co^{III} ion. For a detailed discussion of this rather surprising result see ref.[3][4] Interestingly, $[LRu^{III}Co^{III}Ru^{III}L]^{3+}$ also possesses an S_t = 1 ground state.[14] In both low-spin cobalt(III) containing species no metal-metal bonding is anticipated to play a role due to the

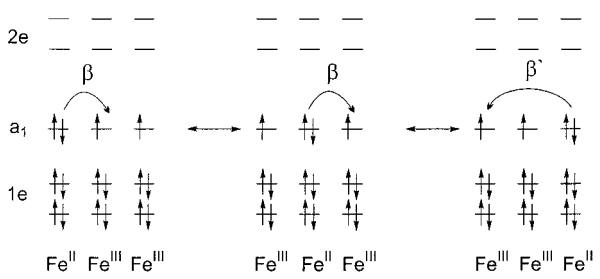

Scheme 3. Electron delocalization in $[\{LFe\}_2Fe]^{2+}$

small size of a cobalt(III) ion (the overlap of a_1 orbitals is very poor).

In the isoelectronic series $[LRuRuRuL]^{2+}$, **1**, $[LFeFeFeL]^{2+}$, $[LRu^{III}Co^{III}Ru^{III}L]^{3+}$, and $[LFe^{III}Co^{III}Fe^{III}L]^{3+}$, each containing 16 valence electrons, the actual ground state correlates with the extent of direct metal−metal bonding, which is significant only in the first two cases, where it yields an $S_t = 0$ ground state. In $[LFeFeFeL]^{2+}$ delocalization of an excess electron over all three iron sites enforces a triplet ground state via double exchange, whereas in $[LRu^{III}Co^{III}Ru^{III}L]^{3+}$ and $[LFe^{III}Co^{III}Fe^{III}L]^{3+}$ there is no metal-metal bonding and the $d^5d^6d^5$ electron configuration is *localized*. Intramolecular spin exchange (ferromagnetic in nature) yields the observed triplet ground state

Experimental Section

Syntheses: The ligand $H_3L \cdot 3\,HPF_6$ was prepared by following the published procedure for $H_3L \cdot 3\,HCl$ by using an HPF_6 solution (ether) instead of HCl in the last step. The synthesis of the mononuclear species $[Fe^{III}L]$ has been described previously.[1]

$[LFeRuFeL](PF_6)_2 \cdot 3\,CH_3OH$ (1): A degassed solution of [FeL] (0.30 g; 0.42 mmol) and $[Ru^{II}Cl_2(dmso)_4]$ (0.20 g; 0.42 mmol) in CH_3OH (50 mL) were heated to reflux under argon for 3 h. To the cooled (20°C) dark brown solution an excess of $NaPF_6$ (1.0 g) dissolved in degassed CH_3OH (25 mL) was added. Within a few hours at 4°C a brown microcrystalline precipitate formed which was collected by filtration (Yield: 0.19 g; 50%). Recrystallization of this material from an acetone-acetonitrile mixture (1:1) produced, after addition of $Na[BPh_4]$, single crystals of $[LFeRuFeL](BPh_4)_2 \cdot CH_3CN \cdot 3\,(CH_3)_2CO$ suitable for X-ray crystallography. − $C_{78}H_{108}N_6S_6RuFe_2(PF_6)_2 \cdot 3\,CH_3OH$: calcd. C 50.95, H 6.30, N 4.37, S 10.01; found C 51.5, H 6.1, N 4.2, S 10.3. − LSIMS *m/z* $[\{LFe\}_2Ru]^+$ 1535; $\{[\{LFe\}_2Ru](PF_6)\}^+$ 1679.6; $[\{LFe\}_2Ru]^{2+}$ 768.3.

$[LFeRuFeL](PF_6)_3$ (2): A degassed solution of [FeL] (0.30 g; 0.42 mmol) and $[RuCl_2(dmso)_4]$ (0.20 g; 0.42 mmol) in CH_3OH (50 mL) was heated to reflux under argon for 3 h. To the cooled (20°C) solution $[NO]BF_4$ (0.05 g; 0.42 mmol) was added and then stirred at 45°C for 3 h. Upon addition of $NaPF_6$ (0.3 g; 1.8 mmol) dissolved in CH_3OH (25 mL) and storage at 4°C for a few hours, a brown precipitate formed (0.15 g). Recrystallization of this material from CH_3CN afforded brown microcrystals of **2**. − $C_{78}H_{108}N_6S_6RuFe_2 \cdot (PF_6)_3$: calcd. C 47.56, H 5.53, N 4.27, S 9.77; found: C 47.2, H 5.5, N 4.1, S 9.5. − ESI (pos. ion) mass spectrometry: $[\{(LFe)_2Ru\}(PF_6)_2]^+$ 1824.2; $[\{(LFe)_2Ru\}(PF_6)]^+$ 1679; $[\{(LFe)_2Ru](PF_6)]^{2+}$ 839.3; $[(LFe)_2Ru]^{2+}$ 766.8.

X-ray Structure Determination: A brown single crystal of $[LFeRuFeL](BPh_4)_2 \cdot CH_3CN \cdot 3\,(CH_3)_2CO$ was mounted on an Enraf−Nonius CAD4 diffractometer in a glass capillary sealed under argon. Graphite-monochromated Mo *Kα* radiation (λ = 0.71073 Å) was used. Cell constants were obtained from a least-squares fit of the setting angles of 25 carefully centered reflections. Intensity data were collected at 100(2) K by using the ω-2θ scan technique, corrected for Lorentz and polarization effects, but no absorption correction was carried out due to the small absorption coefficient.

The Siemens ShelXTL software package[15] was used for solution, refinement, and artwork of the structure which was readily solved and refined by direct methods and difference Fourier techniques. All non-hydrogen atoms were refined anisotropically except the methyl carbon atoms of one disordered acetonitrile and acetone molecule which were isotropically refined on two sites (with occupancy factors 0.5 for each atom). All hydrogen atoms were placed at calculated positions and refined as riding atoms with isotropic displacement parameters. $C_{137}H_{169}B_2Fe_2N_7O_3RuS_6$, M = 2388.54 g mol^{-1}, crystal dimensions 0.49 × 0.35 × 0.21 mm, monoclinic, $Z = 2$, space group $P2_1/c$, a = 12.926(4), b = 15.613(4), c = 31.467(9) Å, β = 90.24(3)°, V = 6350(3) Å^3, $\rho_{calcd.}$ = 1.249 g cm^{-3}, T = 100(2) K, 2θ range = 5.6 to 50.0°, 11387 measured reflections, 11167 unique reflections, 6958 observed reflections [$I > 2\sigma(I)$], 710 parameters, $R_1 = 0.056$, $wR_2 = 0.135$. Further details of the crystal structure determination have been deposited with the Cambridge Crystallographic Data Centre as supplementary publication no. CCDC−125733. Copies of the data can be obtained free of charge on application to CCDC, 12 Union Road, Cambridge CB2 1EZ [Fax: +44 (0)1223/336-033; E-mail: deposit@ccdc.cam.ac.uk].

Physical Measurements: UV/Vis/near-IR spectra of CH_3CN solutions of **1** and **2** were measured on a Perkin−Elmer Lambda 19 spectrophotometer in the range 210−3200 nm at ambient temperature. − Cyclic and square-wave voltammetric and coulometric measurements were performed on EG & G equipment (potentiostat/galvanostat model 273A) on Ar-flushed acetonitrile solutions of samples containing 0.10 M $[N(nBu)_4]PF_6$ as supporting electrolyte at a glassy carbon working electrode and a $Ag/AgNO_3$ reference electrode. Ferrocene (Fc) was added as internal standard; all potentials are referenced vs the Fc^+/Fc couple. − Temperature-dependent magnetic susceptibilities of powdered samples were measured by using a SQUID magnetometer (Quantum Design) at 1.0 T (2.0−300 K). For calculations of the molar magnetic susceptibility, χ_M, the experimental susceptibilities were corrected for the underlying diamagnetism of the sample by using tabulated Pascal's constants. The temperature-independent paramagnetism (χ_{TIP}) was obtained by a fitting procedure. − The X-band EPR spectrum of a frozen solution of **2** was recorded on a Bruker ESP 300E spectrometer equipped with a helium flow cryostat (Oxford Instruments ESR 910). The X-band resonator was a dual-mode cavity (Bruker ER 4116 DM/95). − The Mössbauer spectra were recorded on an alternating constant-acceleration spectrometer. The minimal linewidth was 0.24 mm s^{-1} (full width at half-height). The sample temperature was maintained constant in either an Oxford Variox or an Oxford Mössbauer-Spectromag cryostat. The latter is a split-pair superconducting magnet system for applied fields up to 8 T where the temperature of the sample can be varied in the range 1.5−250 K. The field at the samples is oriented perpendicular to the γ-beam. The $^{57}Co/Rh$ source (1.8 GBq) was positioned at room temperature inside the gap of the magnet system at a zero-field position. Isomer shifts are referenced relative to α-iron metal at 295 K. Details of the analysis within the usual spin Hamiltonian

formalism are given in ref.[3] The depicted fits are the results of an optimization applied simultaneously to the whole series of experimental spectra.

Acknowledgments

We thank the Fonds der Chemischen Industrie for financial support. B. A. is grateful to the Ministry of Education and Culture of Spain for a fellowship.

[1] T. Beissel, K.-S. Bürger, G. Voigt, K. Wieghardt, C. Butzlaff, A. X. Trautwein, *Inorg. Chem.* **1993**, *32*, 124.
[2] T. Beissel, T. Glaser, F. Kesting, K. Wieghardt, B. Nuber, *Inorg. Chem.* **1996**, *35*, 3936.
[3] T. Glaser, T. Beissel, E. Bill, T. Weyhermüller, V. Schünemann, W. Meyer-Klaucke, A. X. Trautwein, K. Wieghardt, *J. Am. Chem. Soc.* **1999**, *121*, 2193.
[4] T. Glaser, K. Wieghardt, in: *Spectroscopic Methods in Bioinorganic Chemistry* (Eds. E. I. Solomon, K. O. Hodgson), ACS Symposium Series, Vol. *692*, 314 (**1998**).
[5] B. Albela, E. Bothe, O. Brosch, K. Mochizuki, T. Weyhermüller, K. Wieghardt, *Inorg. Chem.*, in press.
[6] T. Glaser, F. Kesting, T. Beissel, E. Bill, T. Weyhermüller, W. Meyer-Klaucke, K. Wieghardt, *Inorg. Chem.* **1999**, *38*, 722.
[7] P. Gütlich in: *Mössbauer Spectroscopy*, U. Gonser, Ed., Springer Verlag: Berlin, Heidelberg, New York, 1975.
[8] A. X. Trautwein, E. Bill, E. L. Bominaar, H. Winkler, *Struct. Bonding* **1991**, *78*, 1.
[9] U. Bossek, D. Nühlen, E. Bill, T. Glaser, K. Wieghardt, A. X. Trautwein, *Inorg. Chem.* **1997**, *36*, 2834.
[10] M. B. Robin, P. Day, *Adv. Inorg. Chem. Radiochem.* **1967**, *10*, 247.
[11] A. Bino, F. A. Cotton, *J. Am. Chem. Soc.* **1980**, *102*, 608.
[12] B. E. Bursten, F. A. Cotton, A. Fang, *Inorg. Chem.* **1983**, *22*, 2127.
[13] F. A. Cotton, R. C. Torralba, *Inorg. Chem.* **1991**, *30*, 3293.
[14] O. Brosch, K. Wieghardt, unpublished results.
[15] *ShelXTL V.5*, Siemens Analytical Instruments, Inc., **1994**.

Received June 15, 1999
[I99219]